Apatinib inhibits tumor growth and angiogenesis in PNET models

Shan Wu[1,2,*], Jianjun Zhou[2,*], Jing Guo[3], Zhan Hua[4], Jianchen Li[1] and **Zai Wang[3]**

[1]College of Chemical and Pharmaceutical Engineering, Hebei University of Science and Technology, Shijiazhuang, People's Republic of China
[2]Research Center for Translational Medicine, Cancer Stem Cell Institute, East Hospital, Tongji University School of Medicine, Shanghai, People's Republic of China
[3]Institute of Clinical Medical Sciences, China-Japan Friendship Hospital, Beijing, People's Republic of China
[4]Department of General Surgery, China-Japan Friendship Hospital, Beijing, People's Republic of China

Correspondence should be addressed to Z Hua, J Li or Z Wang: **huazhan@hotmail.com**, **lijianchen152@hotmail.com** or **wzai_163pass@163.com**

*(S Wu and J Zhou contributed equally to this work)

Abstract

Angiogenesis has a pivotal role in the growth and metastasis of pancreatic neuroendocrine tumors (PNETs). Apatinib inhibits angiogenesis as a highly selective KDR inhibitor and has been used to treat advanced gastric cancer and malignancies in clinical settings. However, the efficacy of apatinib in PNETs remains unclear. The aim of this study was to compare the antitumor efficacy of apatinib with that of the standard PNET drug sunitinib in our subcutaneous and liver metastasis models of insulinoma and non-functional PNET. Our results revealed that apatinib had a generally comparable or even superior antitumor effect to that of sunitinib on primary PNET, and it inhibited angiogenesis without directly causing tumor cell cytotoxicity. Apatinib inhibited the tumor in a dose-dependent manner, and the high dose was well tolerated in mice. We also found that the apatinib efficacy in liver metastasis models was cell-type (disease) selective. Although apatinib efficiently inhibited INR1G9-represented non-functional PNET liver metastasis, it led to the emergence of a hypoxic area in the INS-1-represented insulinoma and promoted liver metastasis. Our study demonstrated that apatinib has promise for clinical applications in certain malignant PNETs, and the application of anti-angiogenesis drugs to benign insulinomas may require careful consideration.

Key Words

▶ pancreatic neuroendocrine tumors

▶ angiogenesis

▶ KDR

▶ apatinib

▶ liver metastasis

Introduction

Pancreatic neuroendocrine tumors (PNETs) are a group of rare neoplasms originating from pancreatic endocrine cells (1) that account for 1.3–10.0% of all pancreatic tumors, with an incidence rising to 3.65/100,000 people per year. Sixty-five percent of patients develop distant metastases when diagnosed and have an unfavorable prognosis (2, 3). Currently, the medical treatments of PNETs are limited. Therefore, new drug evaluation is urgently needed. In recent years, several potential therapeutic targets have been proposed, and clinical trials that may bring new treatment options are ongoing (4).

Angiogenesis is indispensable in both tumor growth and metastasis (5). The vascular endothelial growth factor (VEGF) signaling pathway has a critical role in angiogenesis, which indirectly mediates the underlying pathology and subsequent effects on cell proliferation, migration, permeability and survival of the vascular endothelium (6, 7). As a crucial receptor for VEGF, KDR (VEGFR2) stimulates extracellular signal-regulated kinase phosphorylation and proliferation via a protein kinase C-dependent pathway involving activation of PLC-c (8). PNETs are highly vascularized neoplasms

due to overexpression of VEGF (9), particularly in liver metastasis (10). For this reason, sunitinib, a multi-targeted tyrosine kinase receptor inhibitor of VEGFR1-3, platelet-derived growth factor receptor, mast/stem cell growth factor receptor kit, proto-oncogene tyrosine-protein kinase receptor Ret, colony-stimulating factor-1 receptor and Fms-like tyrosine kinase 3 (11), has been proven to be clinically effective in the treatment of PNETs (12). However, serious side effects, which may be caused by the non-specificity of multiple targets (13, 14), may occur in some patients.

In contrast to sunitinib, apatinib is a highly selective inhibitor of KDR tyrosine kinase, with a binding affinity five times that of sunitinib (15). As an antagonist against the ATP site of KDR (16), apatinib blocked the downstream pathway to interrupt angiogenesis in many tumors (10). Apatinib is the first drug in the world that has been approved for patients with advanced gastric carcinoma who do not have further chemotherapy options (6). The drug has also shown promising therapeutic effects against non-triple-negative metastatic breast cancer, advanced non-small-cell lung cancer, gynecological cancer, hepatocellular carcinoma, thyroid cancer and sarcomas in clinical trials (17, 18, 19, 20, 21, 22, 23, 24). However, it is unknown if apatinib is equally effective in PNETs.

The aim of this study was to compare the antitumor efficacy of apatinib with that of the standard PNET drug sunitinib in our subcutaneous and liver metastasis models using two typical types of PNET cells: insulinoma cells, represented by INS-1 (a type of functional PNET), and INR1G9 cells, which are non-functional PNET cells. We found that the PNET inhibition effect of apatinib was generally comparable or even superior to that of sunitinib.

Materials and methods

Substance

The agents used in the present study were apatinib (HengRui Medicine Co. LTD, Jiangsu, China), sunitinib (G1430008, Aladdin, Shanghai, China), antibodies against PECAM1 (CD31) (ab182981, Abcam plc), Hypoxyprobe™-1 Plus Kit (Hypoxyprobe, Inc, USA), Glucagon (sc-13091, Santa Cruz Biotechnology, Inc), Insulin (I2018, Sigma-Aldrich), Pcsk1 (ab5543, Abcam plc), Pcsk2 (ab3533, Abcam plc); Alex Fluor 555 donkey anti-mouse antibody and Alex Fluor 488 donkey anti-rabbit antibody (Invitrogen; Thermo Fisher Scientific, Inc.). All the antibodies were tested previously to ensure

the validation for cross-species. CCK-8 kit (Dojindo Laboratories, Kumamoto, Japan) was used in our study.

Cell culture and reagents

The golden hamster INR1G9 and rat insulinoma INS-1 cells were kindly provided by Dr Haiyan Wang from Division of Clinical Biochemistry, Geneva University Medical Center, Switzerland. INR1G9 were grown in RPMI-1640 medium (Gibco; Thermo Fisher Scientific, Inc.) containing 11.2 mM glucose and supplemented with 5% fetal bovine serum (FBS; Biological Industries Israel BeitHaemek, Kibbutz-BeitHaemek, Israel), 10^5 U/L penicillin and 100 mg/L streptomycin at 37°C with 5% CO_2. INS-1 cells were cultured in RPMI-1640 medium containing 11.2 mM glucose and supplemented with 10% FBS, 50 μM 2-mercap-toethanol, 10^5 U/L penicillin and 100 mg/L streptomycin at 37°C with 5% CO_2. All the experiments were conducted in the exponential phase of cell.

Establishment of EGFP-labeled INR1G9 cells

The lentiviral vector we used was derived from pcDH-EF1-MCS-T2A-puro (SBI). The T2A sequence was replaced with IRES sequence amplified from pIRES2 (Contech) to avoid any addition of extra amino acids to the gene coding sequence inserted in the multiple cloning site (MCS), and the resulted vector was termed as pcDH-EF1-MCS-IRES-puro. For EGFP labeling, *EGFP* gene was amplified from pEGFP-C1 (Contech) and cloned into the MCS of pcDH-EF1-MCS-IRES-puro to generate pcDH-EF1-EGFP-IRES-puro.

For lentivirus generation, 293T cells were seeded 24 h before transfection, which would reach 80% confluence in 10 cm dishes on the day of transfection. Transfection was performed using X-toremifene HP (Roche). Briefly, 10 μg expression vector, 4.5 μg pLP1, 3.5 μg pLP2 and 2.5 μg pVSVG were added into 1 mL opti-MEM (Gibco). Then, 60 μL of transfection regent was added into the mixture and was mixed well. Twenty minutes later, the transfection mixture was added into the culture medium of 293T cells. Then, 12–18 h later, the medium was changed into fresh medium. The supernatant was collected 48 h post transfection, passed through a 0.45 μm filter (Millipore), and then applied to INR1G9 cells with 8 μg/mL polybrene (Sigma). The infected cells were selected with 2 μg/mL puromycin 72 h later; or at this time point, green fluorescence was monitored under inverted fluorescent microscope (BX51, Olympus).

PNET mouse models

Six to eight-week-old female nude mice (Charles River; Beijing, China) weighted 21.0 ± 0.82 g were used in this experiment. Mice were maintained under SPF conditions and were provided with food and tap water *ad libitum*. Mice were acclimatized to standardized laboratory conditions for at least a week prior to experimentation ($24\pm2°C$; $50\pm10\%$ relative humidity; 12 h light–darkness cycles). All animal studies were carried out in strict accordance with the Principles of Laboratory Animal Care and was approved by the Animal Studies Committee of the China-Japan Friendship Hospital (Beijing, China).

For the subcutaneous model, nude mice were inoculated with 1×10^6 INR1G9 or INS-1 cells suspended in 0.1 mL FBS-free culture medium by subcutaneous injection at the right side of the back. Tumor growth was evaluated every other day by measuring of the tumor diameter (mm) along the largest (a) and perpendicular (b) axes, from which the tumor volume (V; mm^3) was calculated according to the formula: $V=0.5\times a\times b^2$. When the tumor volume reached around 100 mm^3, the mice were randomized into experimental groups. Different doses of apatinib and sunitinib, grinded to powder and dissolved in sterile water, were administered once daily by oral gavage for the indicated periods. The weight of mice was also recorded every other day.

For the liver metastasis model, the nude mice were anesthetized with an intraperitoneal injection of 1% pentobarbital sodium (45 mg/kg). The skin was disinfected with 75% alcohol and an oblique incision was made on left side to pull out the spleen. 1×10^6 INR1G9 or INS-1 cells in 25 μL FBS-free culture medium were injected into the spleen using BD insulin syringe until visible splenic capsule swelling. After injection and needle withdrawal, dry cotton swab was used for hemostasis and cell leakage oppression. Then, the spleen was replaced into the abdominal cavity and the skin was sutured. After 2 weeks of injection, apatinib and sunitinib were administered once daily by oral gavage till the mice were killed. Four weeks later, the mice were killed, and the spleens and livers were removed for further analysis.

Immunohistochemical staining

A series of 5 μm sections were obtained from each paraffin block. The deparaffinized sections were pretreated with 10 mM sodium citrate buffer for antigen unmasking, blocked in normal serum, incubated with primary antibodies at 4°C overnight. Sections were incubated with secondary antibody at room temperature for 30 min. Finally, diaminobenzidine tetrachloride was used for color development, and the slides were counterstained with hematoxylin.

Immunofluorescence staining

For immunofluorescence, after fixation with 4% paraformaldehyde for 10 min and permeabilization with 0.1% Triton-100 for 10 min at room temperature, cells were incubated with primary antibodies overnight at 4°C, and then were incubated with second antibodies for 30 min at 37°C. Nuclei were counterstained with DAPI, and then cells were detected under a fluorescent microscope (Olympus Corporation).

RNA extraction and real-time PCR

Total RNA was extracted by TRIzol (Invitrogen) from cells and tumor tissues according to the manufacturer's instructions. The cDNA was synthesized from 2 μg total RNA using reverse transcription kits (TianGen Bio, Inc, Beijing, China). Real-time PCR was performed on an ABI 7500 Real-Time PCR Systems (Applied Biosystems). The PCR conditions were as follows: 50°C incubation for 2 min, 95°C initial denaturation for 10 min, and then 95°C for 15 s, 60°C for 30 s and 72°C for 30 s for 40 cycles. Fluorescence data were collected in the extension step (72°C for 30 s). All reactions were run in triplicates. The housekeeping gene *Actb* for rat cells or *Gapdh* for hamster cells served as an internal control. The primer sequences are shown in Supplementary Table 1 (see section on supplementary data given at the end of this article).

Cell viability assays

Cell viability assays were determined by using Cell Counting Kit-8 (CCK-8) (WST-8, Dojindo, Kumamoto, Japan), according to the supplier recommendations. Cells were cultured in 96-well plates (3×10^3 cells/well). After incubation for 24 h, the cells in various wells were treated with 0, 300, 600, 1200, 2400 nM apatinib diluted in DMSO for the indicated time points, and the cell numbers in wells were measured as the absorbance (450 nm) of reduced WST-8. The WST-8 reagent solution (10 μL) was added to each well of a 96-well microplate containing 100 μL of cells in the culture medium at various wells, and the plate incubated for 3 h at 37°C. Absorbance was then measured at 450 nm using a microplate reader

(Thermo Electron Corporation, Inc., Waltham, MA, USA). All tests were performed in triplicates.

Statistical analysis

Sections showing positive staining were figured in at least six typical fields (×400) and the average percentage of positive cells was calculated with Image-Pro Plus software (Media Cybernetics, Silver Spring, MD, USA). The hemorrhagic and necrotic areas were calculated by SPSS ver.13.0 (SPSS Inc.) and were used for data analysis. The number of liver metastases was assessed by counting surface tumor nodules on the liver with a dissecting microscope (25). Student's t test was used for calculating the significant difference between groups. *$P<0.05$ and **$P<0.01$ were considered significant. All the data were presented as mean±s.e.m.

Results

Establishment of two types of PNET models

The insulinoma and non-functional PNET models were established with INS-1 and INR1G9 cells, respectively. The INS-1 cell line was from an X-ray-induced rat insulinoma, which expressed high levels of insulin and small amounts of glucagon. The establishment of a subcutaneous tumor model has been proven to be accessible (26). With the symptom of hypoglycemia (Fig. 1G), we considered it to be the insulinoma model. The INR1G9 cell line was originally from a single clone of hamster insulinoma. Interestingly, it expressed a high level of glucagon but marginal insulin (Fig. 1A, B and C) and has long been investigated as an *in vitro* model of glucagon secretion (27). In our study, we found that the protein convertases Pcsk1 and Pcsk2 were both expressed in INR1G9 cells, suggesting that it was possible for proglucagon to be dissected into glucagon, GLP-1 and GLP-2 in this cell line (Fig. 1D, E and F). For subcutaneous tumors, although INS-1 xenograft tumors (26) caused severe hypoglycemia, the blood glucose level showed no significant change in INR1G9-tumor-bearing mice (Fig. 1G). Therefore, INR1G9 was considered to be a non-functional PNET model. We established a liver metastases model based on EGFP-labeled INR1G9 cells, which showed obvious metastases in mouse liver after 2 weeks of injection (5/5) (Fig. 1H and I). However, few liver metastases have been observed in INS-1 models, similar to observations in most insulinoma patients (28).
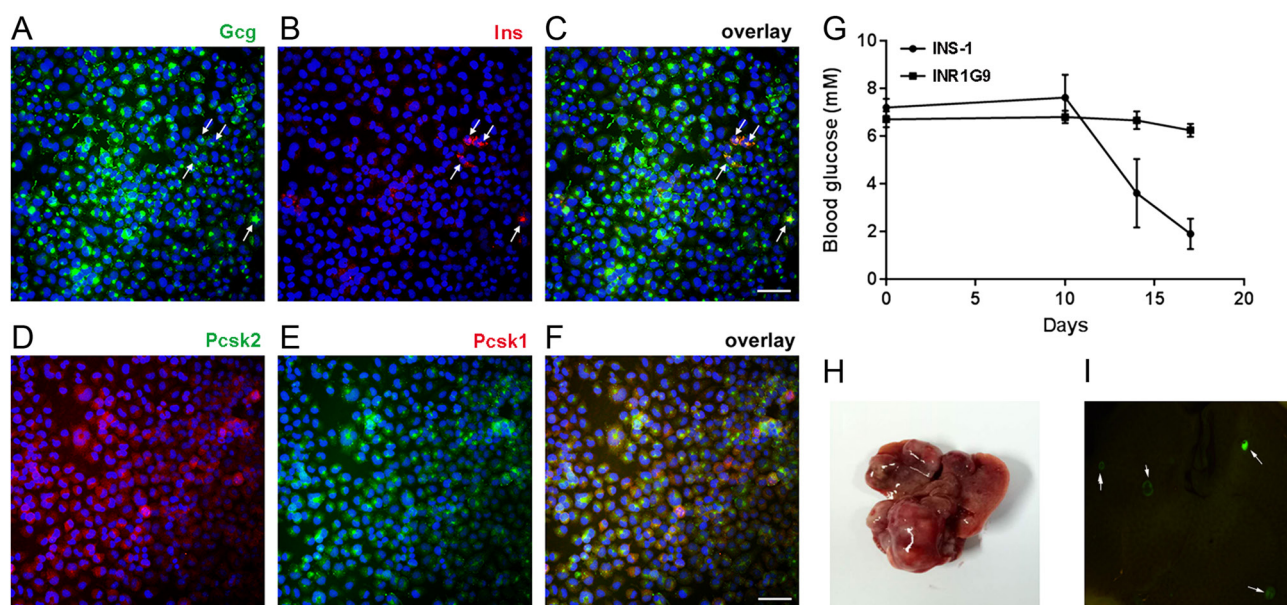
Figure 1

Establishment of PNET models. (A, B, C, D, E and F) Immunofluorescence on INR1G9 cells. (A, B and C) glucagon (green, arrows in (A)) and insulin (red, arrows in (B)); (D, E and F), Pcsk2 (red) and Pcsk1 (green). Nuclei were counterstained with DAPI (blue). Scale bar, 20 µm. (G) The change of blood glucose in nude mice with INR1G9 or INS-1 cells injected subcutaneously. (H and I) Liver metastasis model established by INR1G9 cells. (H) Representative picture of liver with multiple metastases based on INR1G9. (I) Liver metastases with EGFP-labeled INR1G9 cells observed under fluorescent stereomicroscope. The metastatic tumors were indicated by arrows.

Apatinib has no cytotoxicity on INR1G9 and INS-1 cells *in vitro*

It has been previously reported that apatinib has no cytotoxicity on several tumor cell lines, including lung, colon and gastric tumor cells *in vitro*, which hardly express KDR (29, 30), whereas it does inhibit cell proliferation of tumor cells that express KDR (31, 32). To examine the expression of Vegfa and Kdr in INR1G9 or INS-1 cells, we performed real-time RT-PCR. The results showed that INR1G9 did not express Kdr but overexpressed Vegfa compared with BHK cells (Fig. 2A). Similar results were observed in INS-1 cells (Fig. 2C). Consistently, cytotoxicity experiments on INR1G9 and INS-1 cells showed that apatinib had no toxic effect on cell proliferation at a wide range of concentrations from 300 nM to 2400 nM *in vitro* (Fig. 2B and D).

Apatinib shows antitumor efficacy in subcutaneous PNET models

The antitumor potential of apatinib was first evaluated in INR1G9 and INS-1 subcutaneous xenograft models. For both INS-1 and INR1G9 models, once-daily oral administration of apatinib at high (150 mg/kg) or low (50 mg/kg) doses were tested. Although the low dose of apatinib (50 mg/kg) modestly inhibited the growth of tumors, there was no significant difference compared with inhibition in the control group, whereas treatment with a

high dose of apatinib (150 mg/kg) significantly inhibited tumor growth, with the inhibitory effect comparable to that of sunitinib (40 mg/kg) administration alone (Figs 3A and 4A). There was no notable decrease in mice weight receiving different doses of apatinib or sunitinib treatments, which suggested that the high dose of apatinib was well tolerated (Supplementary Fig. 1). In addition, there were significant differences in tumor morphology between the different groups. Compared with the control group in which the tumors were big and had a bloody appearance, the high-dose-treated tumors in the apatinib and sunitinib treatment groups looked smaller and pale (Figs 3C and 4B). Furthermore, the treatment of apatinib in the INS-1 model significantly increased the mice survival rate (Fig. 4D).

Apatinib suppresses tumor angiogenesis *in vivo*

Because apatinib has been shown to target KDR specifically, we investigated the blood vessel formation in INR1G9 and INS-1 tumors. The density of blood vessels in tumors was calculated according to Pecam1 staining (Figs 5C and 6A). Although the low dose of apatinib modestly reduced the vessel density compared with that of the control group ($P<0.05$), treatment with a high dose of apatinib significantly inhibited angiogenesis ($P<0.01$), similar to the sunitinib administration group ($P<0.01$) (Figs 5D and 6C). For INS-1 tumors, we have demonstrated that
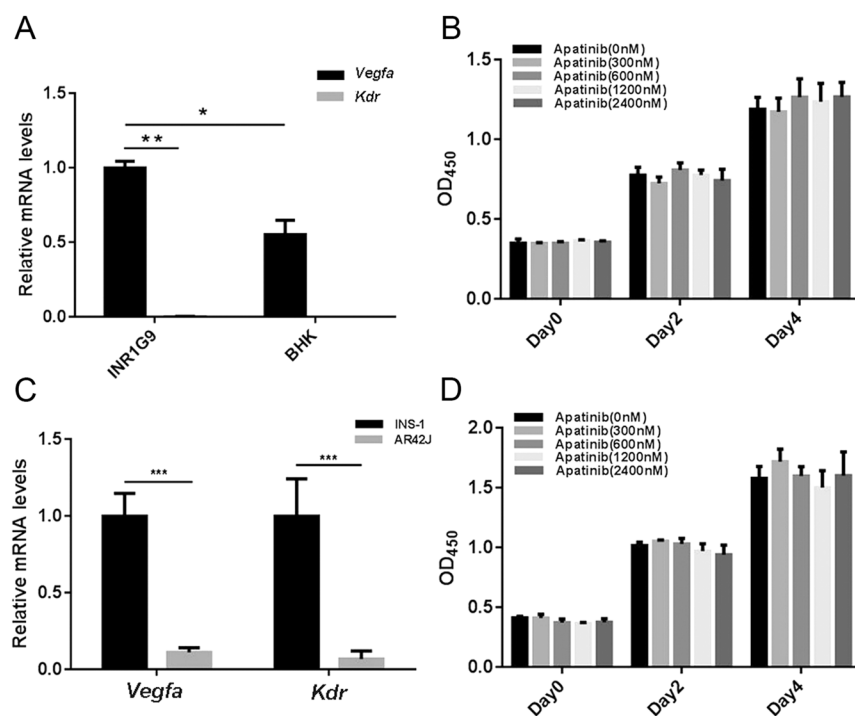
Figure 2

Apatinib showed no cytotoxicity on PNET cells. (A) The mRNA expression levels of *Vegfa* and *Kdr* in INR1G9 and BHK cells. (B) CCK-8 assay performed on INR1G9 cells treated with different doses of apatinib as indicated. (C) The mRNA expression levels of *Vegfa* and *Kdr* in INS-1 and AR42J cells. (D) CCK-8 assay performed on INS-1 cells treated with different doses of apatinib as indicated.
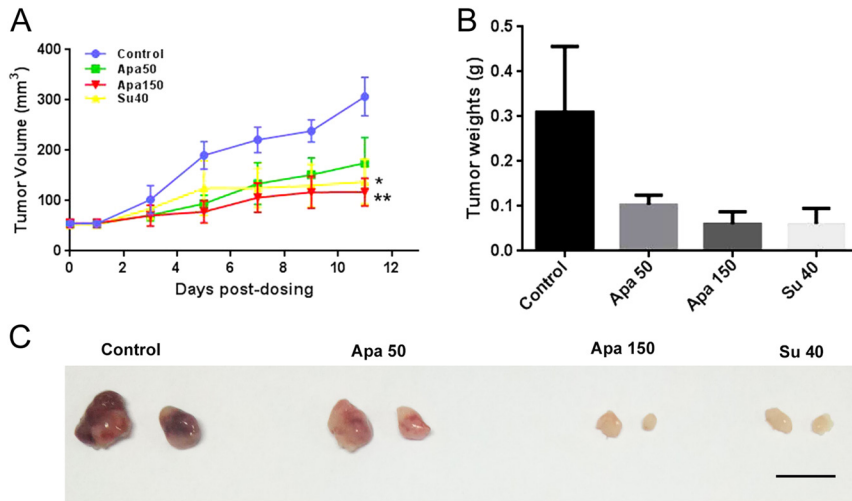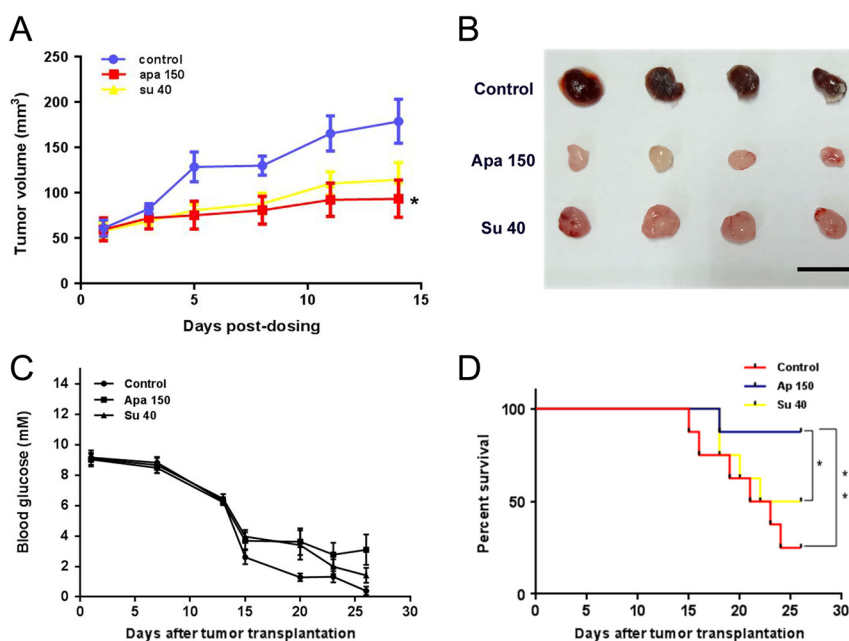
Figure 3

Antitumor activity of apatinib against INR1G9 subcutaneous tumors in nude mice. (A) Tumor volumes measured every other day ($n = 8$). (B) Tumor weights measured after tumor dissection. (C) Representative picture of tumors in four groups. Scale bar, 1 cm. Apa 50, apatinib 50 mg/kg; Apa 150, apatinib 150 mg/kg; Su 40, sunitinib 40 mg/kg.

a special type of hemorrhagic-like region presents as blood-filled caverns with a smooth boundary and unlined by endothelial cells. This pseudo-hemorrhagic region formation is a result of blood vessel dilation followed by endothelial cell detachment (26). In the present study, we found that inhibition of angiogenesis in INS-1 tumors significantly reduced the areas of pseudo-hemorrhagic regions (Fig. 6A and B).

### Apatinib does not affect intra-tumoral hemorrhage and necrosis in the INR-1G9 model

The main reason for necrosis in malignant tumors is the rapid growth of tumor cells without sufficient blood supply. In contrast to INS-1 tumors, INR1G9 tumors contain large amounts of diffusive hemorrhagic regions. The necrotic areas surrounded the hemorrhagic regions along the blood vessels, which suggested that intra-tumoral hemorrhage from the blood vessels interrupted the normal blood supply to the surrounding tumor cells. H&E staining showed that a large area of hemorrhage and necrosis was present in the middle of the untreated tumors, which was absent in the treated groups (Fig. 5A), probably due to the smaller size of the drug-treated tumors. In the treated groups, hemorrhagic and necrotic regions were present along the vessels throughout the tumors, and no differences in the rates of hemorrhage and necrosis were observed between the groups (Fig. 5B),

Figure 4

Antitumor activity of apatinib against INS-1 subcutaneous tumors in nude mice. (A and B) Tumor growth in apatinib- or sunitinib-treated mice ($n = 8$). Experiment was terminated when four mice died in the control group. (A) Tumor volumes measured every other day. (B) Representative picture of tumors in three groups. Scale bar, 1 cm. Apa 150, apatinib 150 mg/kg; Su 40, sunitinib 40 mg/kg. (C and D) Blood glucose and survival rate in apatinib- or sunitinib-treated mice ($n = 8$). Blood glucose was measured at indicated time points (C) and the survival rate (D) was recorded in the same batch of experiment.
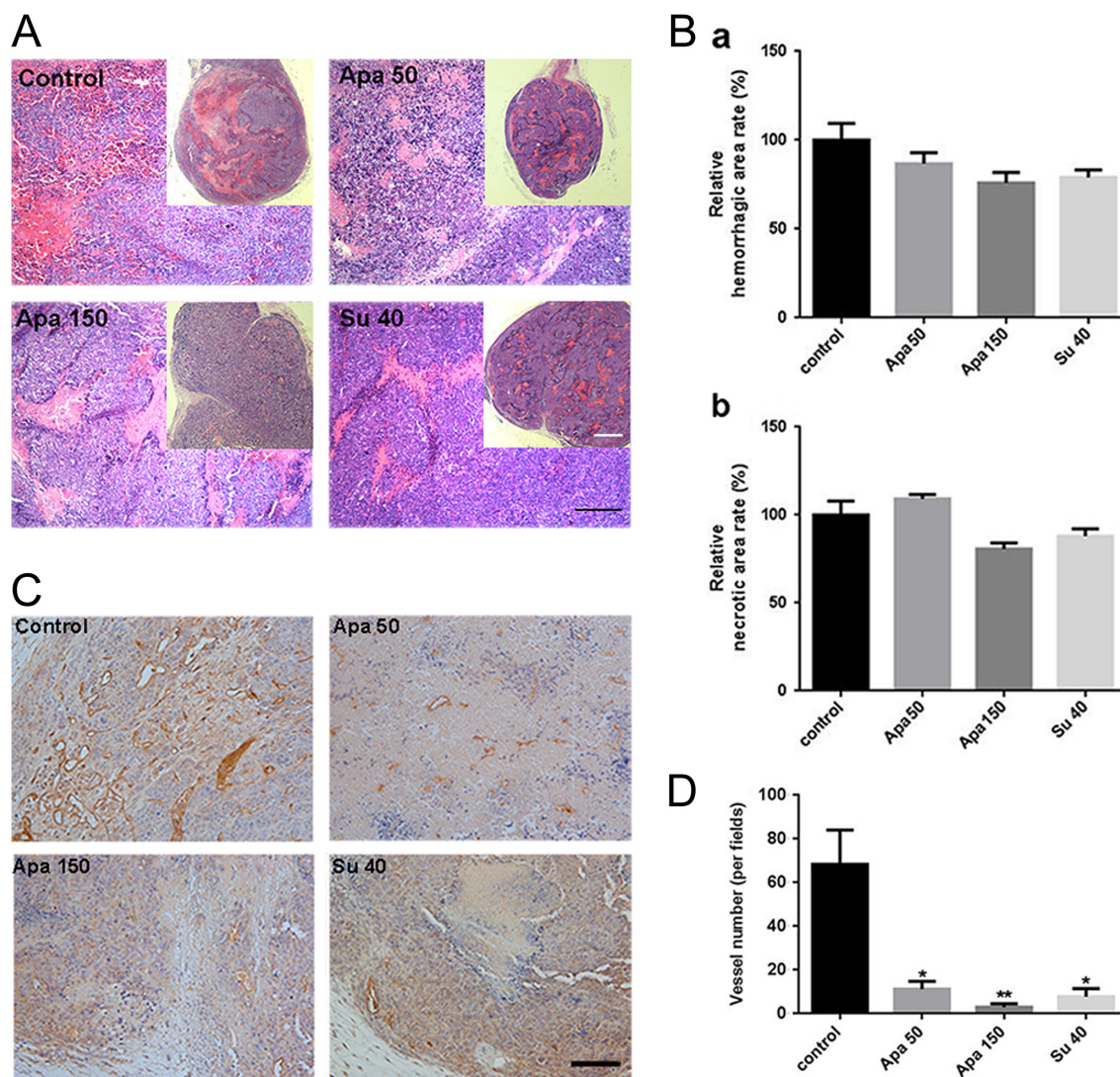
Figure 5
Apatinib reduced vessel density in INR1G9 subcutaneous tumors, but the hemorrhagic and necrotic areas showed no significant changes in tumors. (A) H&E staining of tumors. Scale bar, 200 μm. The full panorama of tumor in each group is at the right corner on each picture. Scale bar, 500 μm. (B) Quantitative analysis of the relative hemorrhagic regions (a) and necrotic regions (b) in (A). (C) Immunohistochemistry of Pecam1 in tumors, scale bar, 200 μm. (D) Quantitative analysis of positive rate of Pecam1 in tumors. Scale bar, 200 μm. Apa 50, apatinib 50 mg/kg; Apa 150, apatinib 150 mg/kg; Su 40, sunitinib 40 mg/kg.

which indicated that although apatinib and sunitinib treatments inhibited angiogenesis, they did not affect the process of hemorrhage.

Apatinib shows superior antitumor efficacy in an INR1G9 liver metastasis model compared with sunitinib

The antitumor efficacy of apatinib was further assessed in the liver metastasis model. The tumor metastases in the apatinib (150 mg/kg)-treated group were significantly decreased ($P < 0.05$ vs control). The inhibitory effect was

even better than that in the sunitinib-treated group according to the area of liver metastases (Fig. 7A and B). The vessel density in the metastatic tumors showed similar results (Fig. 7C).

Anti-angiogenic treatments do not induce hypoxia in INR1G9 tumors but elicit hypoxic areas in INS-1 tumors

It has been reported that hypoxic regions caused by anti-angiogenesis in primary tumors may induce metastasis (33). In the INR1G9 models, there were no significant
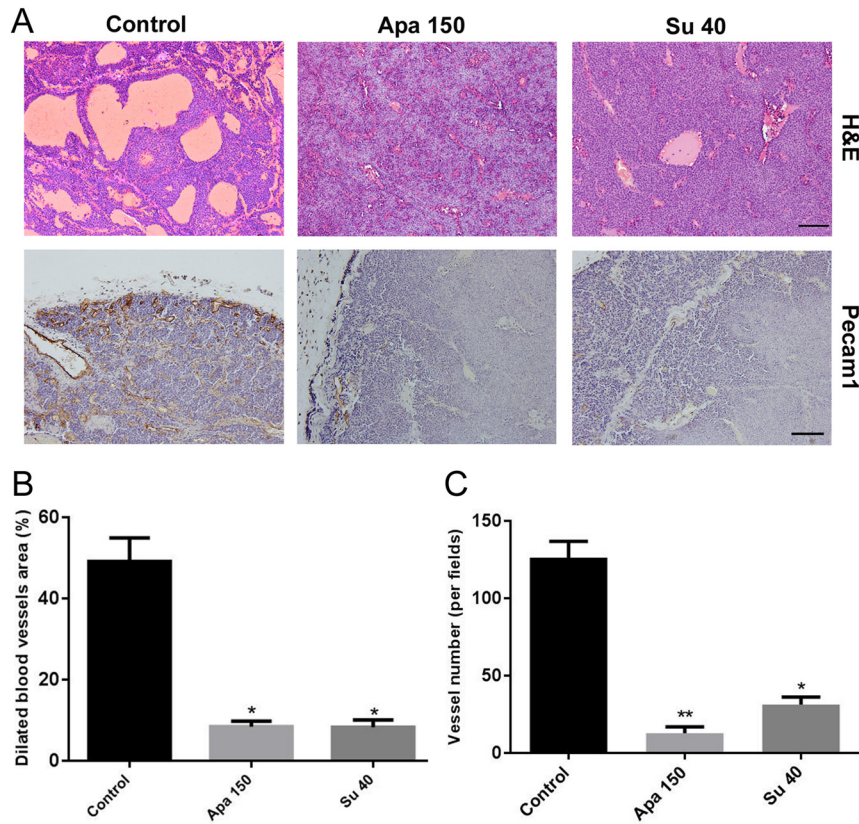
Figure 6
Apatinib reduced the dilated blood vessel area and vessel density in INS-1 subcutaneous tumors. (A) H&E staining (upper panel) and Pecam1 staining (lower panel) of tumors ($n = 8$). (B) Quantitative analysis of the dilated blood vessel area in tumors. (C) Quantitative analysis of the vessel numbers in tumors according to the Pecam1 staining in (A). Scale bars, 200 μm. Apa 50, apatinib 50 mg/kg; Apa 150, apatinib 150 mg/kg; Su 40, sunitinib 40 mg/kg.
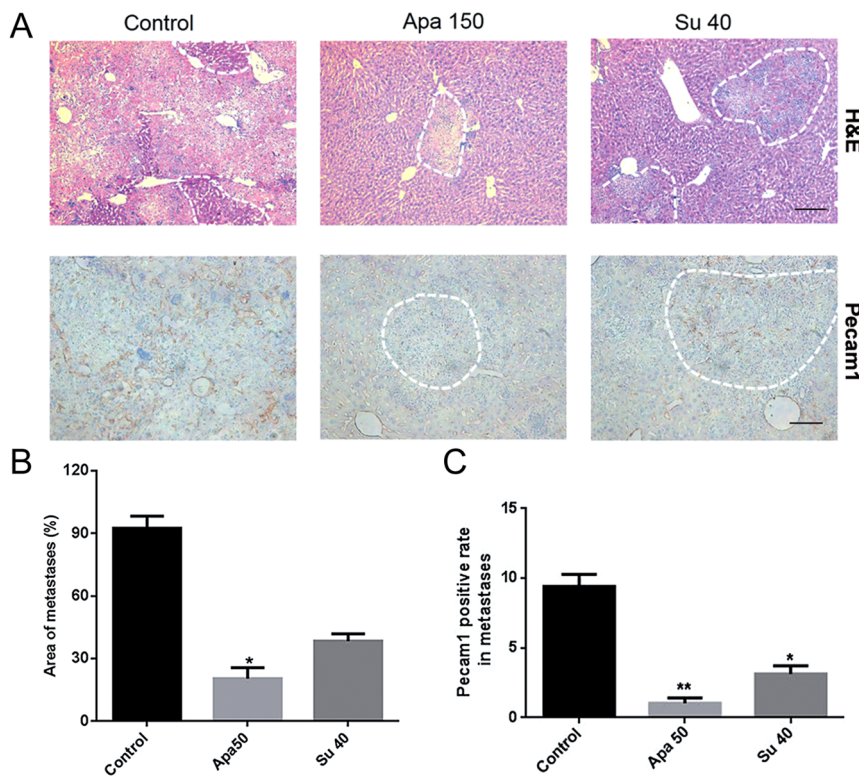
Figure 7
Apatinib inhibited metastases and vessel density in INR1G9 liver metastasis model. (A) Microscopic liver metastases were detected by H&E staining (upper panel) and immunohistochemistry staining of Pecam1 (lower panel) ($n = 8$). The areas of liver metastases were traced out by dotted lines at the edge of tumors. Scale bar, 200 μm. (B) Numbers of liver metastases in different groups as indicated. (C) Pecam1 expression levels in liver metastases in different groups as indicated. Apa 50, apatinib 50 mg/kg; Apa 150, apatinib 150 mg/kg; Su 40, sunitinib 40 mg/kg.

differences in the hypoxic areas in the control and apatinib- or sunitinib-treated groups (Fig. 8A and B). In the INS-1 model, the hypoxic area was markedly induced by treatment with apatinib or sunitinib. Next, we examined whether the induced tumor hypoxia could cause liver metastasis. Although metastasis was hardly detected in the control group, it was detected in some of the apatinib- and sunitinib-treated mice (Fig. 8E and F). These results

indicated that anti-angiogenesis treatment may function differently in tumor metastasis in different models.

Discussion

In this study, we generated insulinoma and non-functional PNET preclinical models based on INR1G9 and INS-1 cells
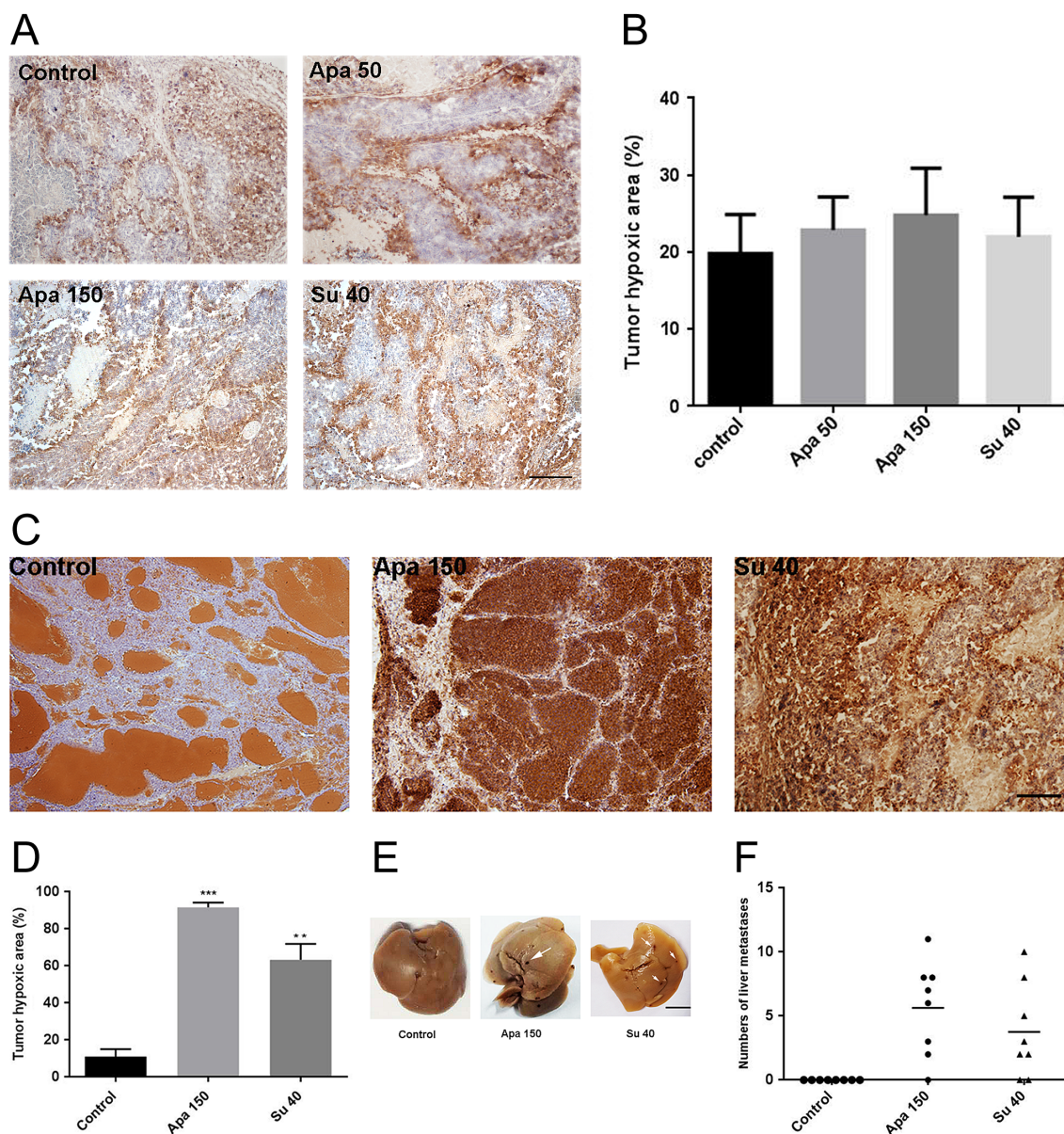
Figure 8

Apatinib promoted liver metastases through increasing hypoxic areas in tumor in INS-1 liver metastasis model. (A) Immunohistochemistry staining for Hypoxyprobe in INR1G9 liver metastases model. Scale bar, 200 μm. (B) Quantitative analysis of tumor hypoxia areas in INR1G9 liver metastases model. (C) Immunohistochemistry staining of Hypoxyprobe in INS-1 tumors. Scale bar, 200 μm. (D) Quantitative analysis of tumor hypoxic areas of INS-1 liver metastases model. (E) Representative picture of livers in INS-1 liver metastasis model. Scale bar, 500 mm. (F) Number of liver metastases in each liver of INS-1 tumor model (*n* = 8). Apa 50, apatinib 50 mg/kg; Apa 150, apatinib 150 mg/kg; Su 40, sunitinib 40 mg/kg.

and compared the antitumor efficacy of apatinib with that of sunitinib in these models. Currently, PNET preclinical models are scarce. The widely used mouse models include RIP-Tag2 mice (34) and MEN1 mutant mice (35), which are genetically engineered models and are time consuming for drug evaluation. Xenograft models based on human PNET cell lines include only BON-1 and QGP-1 cells. However, the mutations identified in RAS and TP53 in both cell lines suggested that they may not represent the majority of clinical PNETs (36). Therefore, the subcutaneous and liver metastasis models of insulinoma and non-functional PNETs presented in this study are valuable for drug evaluation.

PNETs are highly vascularized tumors, and anti-angiogenesis therapy has been applied to PNETs. Sunitinib, one of the angiogenesis-targeted drugs, is the clinical recommendation for PNETs therapy as a multi-target tyrosine kinase inhibitor, but it may cause critical side effects due to the multi-target features (37). Apatinib is a highly selective inhibitor of KDR, with an IC_{50} of $0.001\,\mu M$ vs $0.005\,\mu M$ for sunitinib *in vitro* (15). Additionally, the maximum safe dose for apatinib in clinically approved gastric adenocarcinoma and gastric esophageal cancer treatment is $850\,mg/qd$ (38, 39), whereas for sunitinib, it is only $37.5\,mg/qd$ in PNETs (13). On the basis of the high specificity and high tolerance, we think that apatinib may be a potent anti-PNET drug. In our study, we showed that both sunitinib and apatinib inhibited tumor growth and were tolerated *in vivo*, which demonstrated that apatinib is a promising drug for PNET treatment, similar to sunitinib. Since cell proliferation could not be inhibited by sunitinib or apatinib *in vitro*, the mechanism of the antitumor effect of the drugs appears to not directly target tumor cells but rather angiogenesis.

Since VEGFA regulates not only angiogenesis but also vessel permeability (40), we also observed the hemorrhage regions in the treated tumors. Intra-tumoral hemorrhage is common in PNETs. We have previously demonstrated that the pseudo-hemorrhagic region formation in INS-1 tumors is a result of vessel dilation followed by endothelial cell detachment, which is not relevant to tumor malignancy (26). In the present study, we showed that this pseudo-hemorrhagic region formation could be inhibited by anti-angiogenesis treatments. However, in the INR1G9 tumors, a huge area of diffusive hemorrhage and necrosis coexisted in the middle of tumors, and dispersive hemorrhagic and necrotic regions were present along the blood vessels in the periphery, which was completely different from the condition of INS-1 tumors. We considered that the high leakage property of the blood vessels in INR1G9 cells caused hemorrhaging along the blood vessels, which led to the interruption of blood supply and formation of hypoxia and necrosis around these regions. However, our results showed that there were no significant differences in the regions of hemorrhage, necrosis or hypoxia between the untreated group and apatinib- or sunitinib-treated groups in the INR1G9 models. These data showed that although apatinib and sunitinib inhibited Vegfa-mediated angiogenesis in the INR1G9 tumors, they did not interfere with the hemorrhage process, which might be mediated by signal molecules other than Vegfa (41, 42).

Whether anti-angiogenic drugs can be applied to metastatic PNETs is another issue worth considering. In our liver metastasis models, the antitumor efficacy of apatinib was not consistent in different cell lines. In the INR1G9 cells, which were prone to metastasis without any treatment, both apatinib and sunitinib inhibited the metastasis rate, and apatinib showed an even superior capability to that of sunitinib, suggesting that both drugs may be promising in the treatment of metastatic PNETs. Interestingly, in the INS-1 model, we found that both anti-angiogenesis treatments promoted liver metastasis, with significantly enhanced hypoxic area formation. Since without treatment, there was no liver metastasis observed in the INS-1 model, this insulinoma model might be considered to be a benign tumor model similar to most of the small insulinomas (28). Therefore, our results suggested that although anti-angiogenesis drugs may inhibit metastasis in malignant non-functional PNETs, they may elicit hypoxia and promote metastasis in benign insulinomas. Thus, application of these anti-angiogenesis drugs to benign insulinomas may require careful consideration.

References

1 Halfdanarson TR, Rabe KG, Rubin J & Petersen GM. Pancreatic neuroendocrine tumors (PNETs): incidence, prognosis and recent trend toward improved survival. *Annals of Oncology* 2008 **19** 1727–1733. (https://doi.org/10.1093/annonc/mdn351)

2 Frilling A, Modlin IM, Kidd M, Russell C, Breitenstein S, Salem R, Kwekkeboom D, Lau WY, Klersy C, Vilgrain V, *et al*. Recommendations for management of patients with neuroendocrine liver metastases. *Lancet Oncology* 2014 **15** e8–e21. (https://doi.org/10.1016/S1470-2045(13)70362-0)

3 Hamerlik P, Lathia JD, Rasmussen R, Wu Q, Bartkova J, Lee M, Moudry P, Bartek J Jr, Fischer W, Lukas J, *et al*. Autocrine VEGF-VEGFR2-Neuropilin-1 signaling promotes glioma stem-like cell viability and tumor growth. *Journal of Experimental Medicine* 2012 **209** 507–520. (https://doi.org/10.1084/jem.20111424)

4 Berardi R, Morgese F, Torniai M, Savini A, Partelli S, Rinaldi S, Caramanti M, Ferrini C, Falconi M & Cascinu S. Medical treatment for gastro-entero-pancreatic neuroendocrine tumours. *World Journal of Gastrointestinal Oncology* 2016 **8** 389–401. (https://doi.org/10.4251/wjgo.v8.i4.389)

5 Carmeliet P & Jain RK. Angiogenesis in cancer and other diseases. *Nature* 2000 **407** 249–257. (https://doi.org/10.1038/35025220)

6 Li J, Qin S, Xu J, Guo W, Xiong J, Bai Y, Sun G, Yang Y, Wang L, Xu N, *et al*. Apatinib for chemotherapy-refractory advanced metastatic gastric cancer: results from a randomized, placebo-controlled, parallel-arm, phase II trial. *Journal of Clinical Oncology* 2013 **31** 3219–3225. (https://doi.org/10.1200/JCO.2013.48.8585)

7 Zhang H. Apatinib for molecular targeted therapy in tumor. *Drug Design Development and Therapy* 2015 **9** 6075–6081. (https://doi.org/10.2147/DDDT.S97235)

8 Takahashi T, Yamaguchi S, Chida K & Shibuya M. A single autophosphorylation site on KDR/Flk-1 is essential for VEGF-A-dependent activation of PLC-gamma and DNA synthesis in vascular endothelial cells. *EMBO Journal* 2001 **20** 2768–2778. (https://doi.org/10.1093/emboj/20.11.2768)

9 Capozzi M, Von Arx C, Divitiis DE, Ottaiano A, Tatangelo F, Romano GM & Tafuto S. Antiangiogenic therapy in pancreatic neuroendocrine tumors. *Anticancer Research* 2016 **36** 5025–5030. (https://doi.org/10.21873/anticanres.11071)

10 Hori T, Takaori K & Uemoto S. Pancreatic neuroendocrine tumor accompanied with multiple liver metastases. *World Journal of Hepatology* 2014 **6** 596–600. (https://doi.org/10.4254/wjh.v6.i8.596)

11 Abrams TJ, Lee LB, Murray LJ, Pryer NK & Cherrington JM. SU11248 inhibits KIT and platelet-derived growth factor receptor beta in preclinical models of human small cell lung cancer. *Molecular Cancer Therapeutics* 2003 **2** 471–478.

12 Blumenthal GM, Cortazar P, Zhang JJ, Tang S, Sridhara R, Murgo A, Justice R & Pazdur R. FDA approval summary: sunitinib for the treatment of progressive well-differentiated locally advanced or metastatic pancreatic neuroendocrine tumors. *Oncologist* 2012 **17** 1108–1113. (https://doi.org/10.1634/theoncologist.2012-0044)

13 Valle JW, Faivre S, Hubner RA, Grande E & Raymond E. Practical management of sunitinib toxicities in the treatment of pancreatic neuroendocrine tumors. *Cancer Treatment Reviews* 2014 **40** 1230–1238. (https://doi.org/10.1016/j.ctrv.2014.09.001)

14 Escudier B, Porta C, Bono P, Powles T, Eisen T, Sternberg CN, Gschwend JE, De Giorgi U, Parikh O, Hawkins R, *et al*. Randomized, controlled, double-blind, cross-over trial assessing treatment preference for pazopanib versus sunitinib in patients with metastatic renal cell carcinoma: PISCES Study. *Journal of Clinical Oncology* 2014 **32** 1412–1418. (https://doi.org/10.1200/JCO.2013.50.8267)

15 Mendel DB, Laird AD, Xin X, Louie SG, Christensen JG, Li G, Schreck RE, Abrams TJ, Ngai TJ, Lee LB, *et al*. In vivo antitumor activity of SU11248, a novel tyrosine kinase inhibitor targeting vascular endothelial growth factor and platelet-derived growth factor receptors: determination of a pharmacokinetic/pharmacodynamic relationship. *Clinical Cancer Research* 2003 **9** 327–337.

16 Holmes K, Roberts OL, Thomas AM & Cross MJ. Vascular endothelial growth factor receptor-2: structure, function, intracellular signalling and therapeutic inhibition. *Cellular Signalling* 2007 **19** 2003–2012. (https://doi.org/10.1016/j.cellsig.2007.05.013)

17 Hu X, Cao J, Hu W, Wu C, Pan Y, Cai L, Tong Z, Wang S, Li J, Wang Z, *et al*. Multicenter phase II study of apatinib in non-triple-negative metastatic breast cancer. *BMC Cancer* 2014 **14** 820. (https://doi.org/10.1186/1471-2407-14-820)

18 Langer CJ, Mok T & Postmus PE. Targeted agents in the third-/fourth-line treatment of patients with advanced (stage III/IV) non-small cell lung cancer (NSCLC). *Cancer Treatment Reviews* 2013 **39** 252–260. (https://doi.org/10.1016/j.ctrv.2012.05.003)

19 Aoyama T & Yoshikawa T. Targeted therapy: apatinib – new third-line option for refractory gastric or GEJ cancer. *Nature Reviews Clinical Oncology* 2016 **13** 268–270. (https://doi.org/10.1038/nrclinonc.2016.53)

20 Geng R & Li J. Apatinib for the treatment of gastric cancer. *Expert Opinion on Pharmacotherapy* 2015 **16** 117–122. (https://doi.org/10.1517/14656566.2015.981526)

21 Xie C, Su M & Jin X. Apatinib as a salvage treatment in gynecologic cancer patients failed from two or more lines of prior chemotherapy. *Journal of Clinical Oncology* 2017 **35** e17009–e17009. (https://doi.org/10.1200/JCO.2017.35.15_suppl.e17009)

22 Qin S. Apatinib in chinese patients with advanced hepatocellular carcinoma: a phase II randomized, open-label trial. *Journal of Clinical Oncology* 2014 **32** 4019–4019.

23 Yang W, Zhu B, Li J, Xie Q, Diao L & Gai L. Response of advanced soft tissue Sarcoma to apatinib: a retrospective analysis. *Journal of Clinical Oncology* 2017 **35** e22502–e22502.

24 Zhang X, Wang C & Lin Y. Pilot dose comparison of apatinib in Chinese patients with progressive radioiodine-refractory differentiated thyroid cancer. *Journal of Clinical Endocrinology and Metabolism* 2018 **103** 3640–3646. (https://doi.org/10.1210/jc.2018-00381)

25 Yang W, Li H, Mayhew E, Mellon J, Chen PW & Niederkorn JY. NKT cell exacerbation of liver metastases arising from melanomas transplanted into either the eyes or spleens of mice. *Investigative Ophthalmology and Visual Science* 2011 **52** 3094–3102. (https://doi.org/10.1167/iovs.10-7067)

26 Wang Z, Peng L, Song YL, Xu S, Hua Z, Fang N, Zhai M, Liu H, Fang Q, Deng T, *et al*. Pseudo-hemorrhagic region formation in pancreatic neuroendocrine tumors is a result of blood vessel dilation followed by endothelial cell detachment. *Oncology Letters* 2018 **15** 4255–4261. (https://doi.org/10.3892/ol.2018.7840)

27 Mildner M, Muller-Fielitz H, Stolting I, Johren O, Steckelings M & Raasch W. Glucagon increase after chronic AT1 blockade is more likely related to an indirect leptin-dependent than to a pancreatic alpha-cell-dependent mechanism. *Naunyn-Schmiedeberg's Archives of*

Pharmacology 2017 **390** 505–518. (https://doi.org/10.1007/s00210-017-1346-7)

28 Lewis A, Li D, Williams J & Singh G. Pancreatic neuroendocrine tumors: state-of-the-art diagnosis and management. *Oncology* 2017 **31** e1–e12.

29 Tian S, Quan H, Xie C, Guo H, Lu F, Xu Y, Li J & Lou L. YN968D1 is a novel and selective inhibitor of vascular endothelial growth factor receptor-2 tyrosine kinase with potent activity in vitro and in vivo. *Cancer Science* 2011 **102** 1374–1380. (https://doi.org/10.1111/j.1349-7006.2011.01939.x)

30 Lee HJ, Moon JY & Baek SW. Is treatment-emergent toxicity a biomarker of efficacy of apatinib in gastric cancer? *Journal of Clinical Oncology* 2016 **34** 3823. (https://doi.org/10.1200/JCO.2016.68.8663)

31 Li X, Xu A, Li H, Zhang B, Cao B & Huang J. Novel role of apatinib as a multi-target RTK inhibitor in the direct suppression of hepatocellular carcinoma cells. *Biochimica et Biophysica Acta* 2018 **1864** 1693–1701. (https://doi.org/10.1016/j.bbadis.2018.02.014)

32 Peng S, Zhang Y, Peng H, Ke Z, Xu L, Su T, Tsung A, Tohme S, Huang H, Zhang Q, *et al*. Intracellular autocrine VEGF signaling promotes EBDC cell proliferation, which can be inhibited by Apatinib. *Cancer Letters* 2016 **373** 193–202. (https://doi.org/10.1016/j.canlet.2016.01.015)

33 Pennacchietti S, Michieli P, Galluzzo M, Mazzone M, Giordano S & Comoglio PM. Hypoxia promotes invasive growth by transcriptional activation of the met protooncogene. *Cancer Cell* 2003 **3** 347–361. (https://doi.org/10.1016/S1535-6108(03)00085-0)

34 Hanahan D. Heritable formation of pancreatic beta-cell tumours in transgenic mice expressing recombinant insulin/simian virus 40 oncogenes. *Nature* 1985 **315** 115–122. (https://doi.org/10.1038/315115a0)

35 Bertolino P, Tong WM, Galendo D, Wang ZQ & Zhang CX Heterozygous Men1 mutant mice develop a range of endocrine tumors mimicking multiple endocrine neoplasia type 1. *Molecular*

Endocrinology 2003 **17** 1880–1892. (https://doi.org/10.1210/me.2003-0154)

36 Vandamme T, Peeters M, Dogan F, Pauwels P, Van Assche E, Beyens M, Mortier G, Vandeweyer G, de Herder W, Van Camp G, *et al*. Whole-exome characterization of pancreatic neuroendocrine tumor cell lines BON-1 and QGP-1. *Journal of Molecular Endocrinology* 2015 **54** 137–147. (https://doi.org/10.1530/JME-14-0304)

37 Faivre S, Demetri G, Sargent W & Raymond E. Molecular basis for sunitinib efficacy and future clinical development. *Nature Reviews Drug Discovery* 2007 **6** 734–745. (https://doi.org/10.1038/nrd2380)

38 Pasini F, Fraccon AP, Modena Y, Bencivenga M, Giacopuzzi S, La Russa F, Gusella M & de Manzoni G. Targeted therapies for advanced and metastatic adenocarcinoma of the gastroesophageal junction: is there something new? *Gastric Cancer* 2017 **20** 31–42. (https://doi.org/10.1007/s10120-016-0626-0)

39 Li J, Qin S, Xu J, Xiong J, Wu C, Bai Y, Liu W, Tong J, Liu Y, Xu R, *et al*. Randomized, double-blind, placebo-controlled phase III trial of apatinib in patients with chemotherapy-refractory advanced or metastatic adenocarcinoma of the stomach or gastroesophageal junction. *Journal of Clinical Oncology* 2016 **34** 1448–1454. (https://doi.org/10.1200/JCO.2015.63.5995)

40 Dvorak HF. Vascular permeability factor/vascular endothelial growth factor: a critical cytokine in tumor angiogenesis and a potential target for diagnosis and therapy. *Journal of Clinical Oncology* 2002 **20** 4368–4380. (https://doi.org/10.1200/JCO.2002.10.088)

41 Roberts WG & Palade GE. Increased microvascular permeability and endothelial fenestration induced by vascular endothelial growth factor. *Journal of Cell Science* 1995 **108** 2369–2379.

42 Qin L, Zhao D, Xu J, Ren X, Terwilliger EF, Parangi S, Lawler J, Dvorak HF & Zeng H. The vascular permeabilizing factors histamine and serotonin induce angiogenesis through TR3/Nur77 and subsequently truncate it through thrombospondin-1. *Blood* 2013 **121** 2154–2164. (https://doi.org/10.1182/blood-2012-07-443903)